PERGAMON

Journal of Structural Geology 24 (2002) 1925–1936

JOURNAL OF STRUCTURAL GEOLOGY

www.elsevier.com/locate/jstrugeo

Behaviour of a rupture of the 21 June 2000 earthquake in South Iceland as revealed in an asphalted car park

Jacques Angelier*, Françoise Bergerat

Séismotectonique et Tectonophysique, ESA 7072, University P. & M. Curie, Boîte 129, 4, place Jussieu, 75252 Paris cedex 05, France

Received 20 February 2001; received in revised form 2 December 2001; accepted 3 January 2002

Abstract

A major earthquake ($M = 6.6$) occurred on 21 June 2000, in South Iceland. This paper presents an unusual example of left-lateral strike-slip displacement recorded in a newly asphalted car park surface through a mechanically consistent pattern of open fissures and pressure ridges resulting from simple shear and rotation. Measurement of these features allows accurate reconstruction of the local deformation. The behaviour of the asphalt layer resembles that of analogue physical models, especially in terms of rotations induced by shear deformation. It is finally shown that through a wide range of scales some basic patterns associating rotation and opposite senses of strike-slip exist in the South Iceland Seismic Zone.

Keywords: Earthquake; Left-lateral strike-slip displacement; Deformation; Rupture trace; Transform fault

1. Introduction

Two major earthquakes occurred in southern Iceland on 17 and 21 June 2000. The surface wave and moment magnitudes were $M_s = 6.6$ and $M_w = 6.4$ in both these cases. Detailed information about these earthquakes has been put on several Internet sites (Icelandic Meteorological Office, 2000; National Energy Authority of Iceland, 2000; University of Iceland, 2000). These two earthquakes were strike-slip in type (Stefánsson et al., 2000), related to the seismotectonic behaviour of the South Iceland Seismic Zone. This major structure of southwestern Iceland is an E–W-trending, left-lateral transform zone (Ward, 1971) that connects the Reykjanes segment of the Mid-Atlantic Ridge and the rift of eastern Iceland (Fig. 1a).

We aim first to describe an unusual example of left-lateral strike-slip displacement of the 21 June earthquake, recorded in a newly asphalted car park surface. A recent paper in this journal (Roberts, 2000) highlighted the potential of such artificial asphalt layers to record evidence of deformation. We demonstrate that careful mapping of such human-built surfaces cut by an earthquake rupture trace allows accurate reconstruction of the local deformation. The second aim of this paper consists of drawing the reader's attention to the significance of these earthquake traces, in the context of the left-lateral transform motion along the South Iceland Seismic Zone. This is done in terms of both the structure and the deformation, at contrasting spatial scales. Concerning the general structure and mechanisms of the South Iceland Seismic Zone, the reader is referred to other papers (e.g. Einarsson et al., 1981; Einarsson, 1991; Gudmundsson and Brynjolfsson, 1993; Gudmundsson, 1995; Passerini et al., 1997; Bergerat et al., 1999; Bergerat and Angelier, 2000).

This paper presents mapping, measurements and reconstruction of co-seismic deformation recorded along the Road N°1 of Iceland near Bitra, across the 21 June rupture trace of the Hestfjall Fault (Fig. 1b and c). When our field work was carried out, about one month after the earthquake, the rupture traces were still preserved and clearly observable in the asphalt layer of the car park area.

2. Observed structures

The 21 June earthquake left spectacular traces in the grassy soils near a summerhouse named Bitra, south of the main road (Iceland n°1) from Reykjavik to southeastern Iceland. En échelon fissures (Fig. 2) and push-up structures indicate left-lateral strike-slip in the WSW–ENE direction (N50-60°E). The area described in this paper is a few hundred metres to the ENE of the summerhouse, on the northern edge of the main road (63°57′N and 20°42′W).

The car park area is about 100 m long in the E–W direction, parallel to the main road (Fig. 3a). The brittle features recorded in the horizontal asphalt layer belong to three

* Corresponding author. Fax: +33-1-44-27-50-85.
E-mail address: jacques.angelier@lgs.jussieu.fr (J. Angelier).

0191-8141/02/$ - see front matter
PII: S0191-8141(02)00007-X

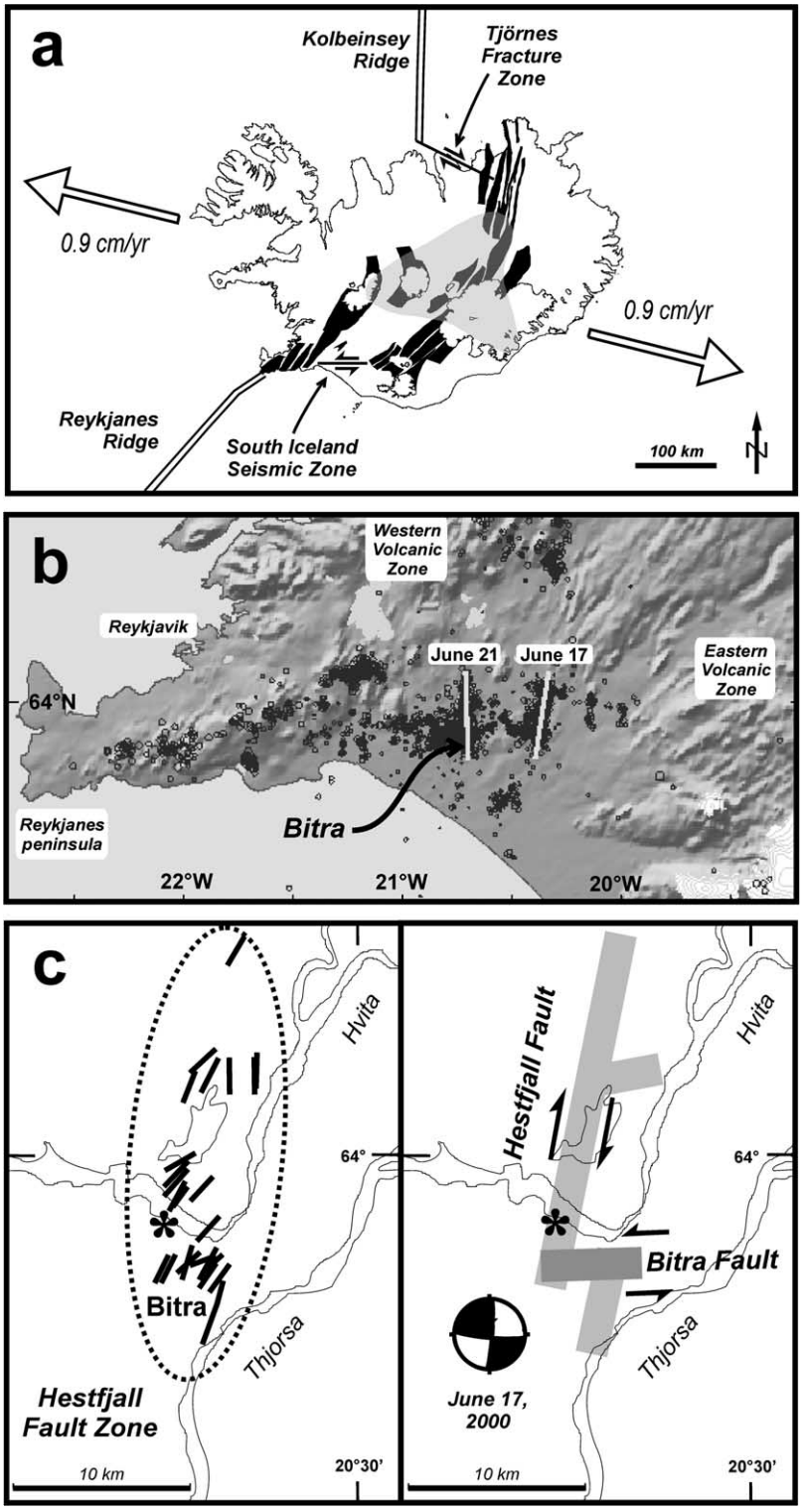

Fig. 1. The South Iceland Seismic Zone and the 17 and 21 June 2000 earthquakes. (a) Geodynamic setting of Iceland. Mid-Atlantic ridge as double line, Icelandic rift zones in black (left white when covered by glaciers), apex of thermal anomaly in light grey, plate divergence indicated by open arrows. (b) Main fault traces and aftershocks of the 17 and 21 June 2000 earthquakes (modified after Stefánsson et al., 2000). Location of the area studied (Bitra) indicated. White lines refer to alignments of earthquake epicentres, not to surface traces. (c) Surface traces (thick black lines) of the 21 June 2000 earthquake, after the National Energy Authority of Iceland (Orkustofnun), 2000. Epicentre as asterisk. Main faults in grey (Bitra Fault in dark grey). Earthquake mechanism added as 'beachball' stereoplot.

Fig. 2. Rupture trace of the 21 June earthquake near Bitra. En échelon fissures and small push-ups indicate left-lateral motion. The car park area analysed in this paper is located to the ENE, in the background near the upper-right of the photograph.

types: open fissures, pressure ridges and left-lateral strike-slip fractures (Fig. 4). Some open fissures show relative displacements that progressively decrease from one edge of the asphalt layer towards a point where the fracture disappears near the opposite edge (Fig. 4a). This is also the case for some pressure ridges (Fig. 4b). A zigzag fracture shows a strike-slip segment that connects two open gashes (Fig. 4c).

Concerning the data collection and the method, our mapping was performed with a Trimble GPS Pathfinder Pro XRS differential system and accurate measurements of characteristic features were carried out with a compass and a metric tape. At many measurement points along all the fracture lines, we determined the relative displacement vectors in azimuth and length. The comparison between these vectors indicated that several portions of the car park area behaved as rigid plates undergoing minor rotation during the earthquake. This conclusion was supported by the absence of observable deformation inside these asphalt plates. It is also supported by the geometrical distribution of relative displacement vectors across each major fracture, consistent with a rigid rotation pattern. In other words, these vectors approximately tangent concentric circles, with amplitudes proportional to radius, which enabled us to locate the rotation pole and determine the rotation angle for each pair of adjacent asphalt plates in the car park. The co-seismic relative displacements between these asphalt plates separated by zones of opening, shortening and simple shear were thus reconstituted through mapping and determination of displacement vectors at asphalt plate boundaries, as discussed in the next section of this paper.

As compared with the earthquake rupture traces in the natural ground surface, these fractures, albeit less spectacular (compare Figs. 2 and 4), allowed accurate reconstruction of the deformation. As Fig. 3a indicates, very little brittle deformation affected the main road and the main car park area. The rupture traces concentrated in the three asphalted access roads which connect the car park and the road. This is not surprising because, near Bitra, the fault trace trends ENE–WSW and the rupture of the 21 June 2000 earthquake essentially propagated between the E–W main road and the car park area (Fig. 3b). Evidence of surface ruptures was present in the soil and the gravel layer, but did not allow the quantification of the deformation at the Bitra car park area. Note that quantification could be done in grassy soils at other sites of the 17 and 21 June 2000 rupture traces (Bergerat and Angelier, 2001).

The orientation of each brittle feature as a function of type (dilation, shortening or strike-slip) deserves particular attention as a key to the rupture mechanism, so the viewlines for all the photographs shown in Figs. 4 and 5 are indicated by open arrows in Fig. 3b. Note that typical open fissures strike NE–SW (Fig. 4a), whereas pressure ridges generally strike NW–SE (Fig. 4b). This pattern is compatible with the WSW–ENE general orientation of the left-lateral rupture trace near the Bitra summerhouse (Fig. 2) and the E–W strike of the left-lateral shear in the asphalt layer of the car park area (Fig. 4c). All these orientations of brittle structures are consistent with NE–SW compression and NW–SE extension.

Rupture traces were observed at three sub-sites, which correspond to the three access roads of the car park area (Fig. 3). Although both the open fissures and the pressure ridges were observed at these three localities, their relative abundance and size vary. The central access road (Fig. 5a), which trends N–S, is affected by two open fissures and two pressure ridges or highs. The eastern access road shows large open fissures and short pressure ridges (Fig. 5b): the open fissures are more abundant and accomplish more strain than the pressure ridges (Fig. 4a and c). In contrast, well-developed pressure ridges affect the western access road (Fig. 5c); these pressure ridges are composed of thrusts and folds in the asphalt layer (Figs. 4b and 5c).

Left-lateral shear was observed along a straight, E–W-trending line between the eastern access road and the car park area (Figs. 4c and 5b). This line coincides with a pre-existing junction between two asphalt surfaces, made during the car park construction. During the earthquake,

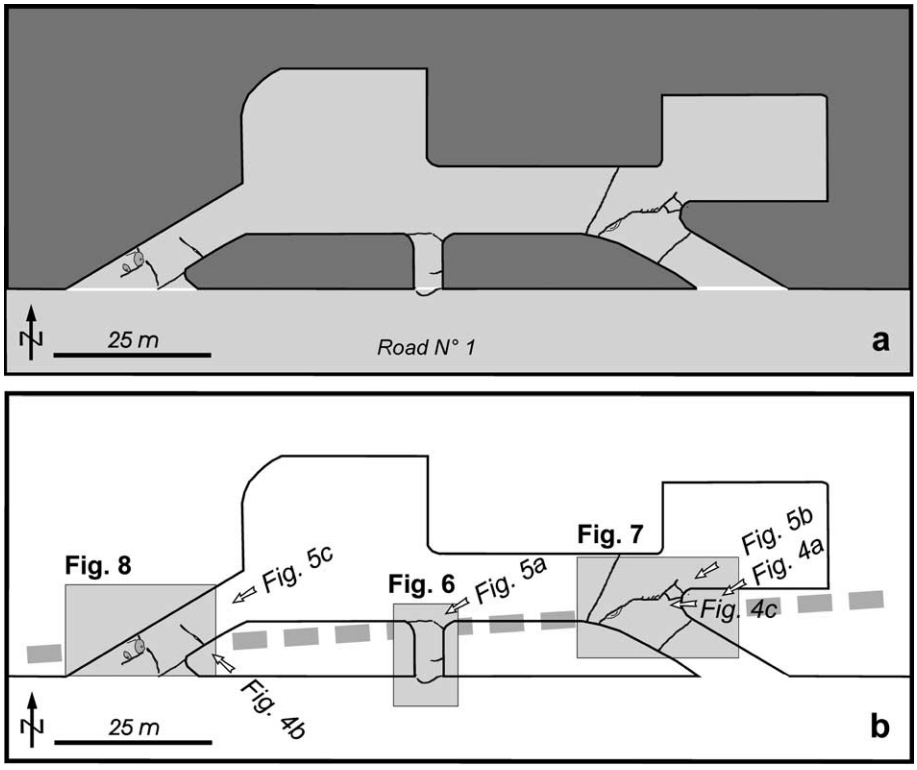

Fig. 3. Map of the car park area near Bitra. (a) General map obtained with a GPS differential system. Grassy soil in dark grey, asphalted areas in light grey, fractures as thin lines. (b) Location of subsequent figures. Mapped sub-areas shaded with figure references in bold characters. Photographs located with open arrows indicating viewlines and references to figures in italic. Fault trace of the 21 June 2000 earthquake as grey dashed line.

the left-lateral slip locally concentrated along this line of mechanical weakness in the asphalt cover so that this slip trace can be regarded as an inherited feature. As Fig. 5b demonstrates, the same E–W line of mechanical weakness also behaved as an open fissure at its eastern tip, so that with the main NE–SW open fissure it defines a triangular area where two parallel pressure ridges trend NW–SE and accommodate shortening (in the foreground of Fig. 5b). In addition, elliptical troughs resulted from the co-seismic collapse of small underground cavities (e.g. a drainage pipe), and are not suitable strain indicators.

The three access roads display contrasting orientations (Fig. 3). The relative importance of open fissures and pressure ridges vary as noted above. For this reason, these three

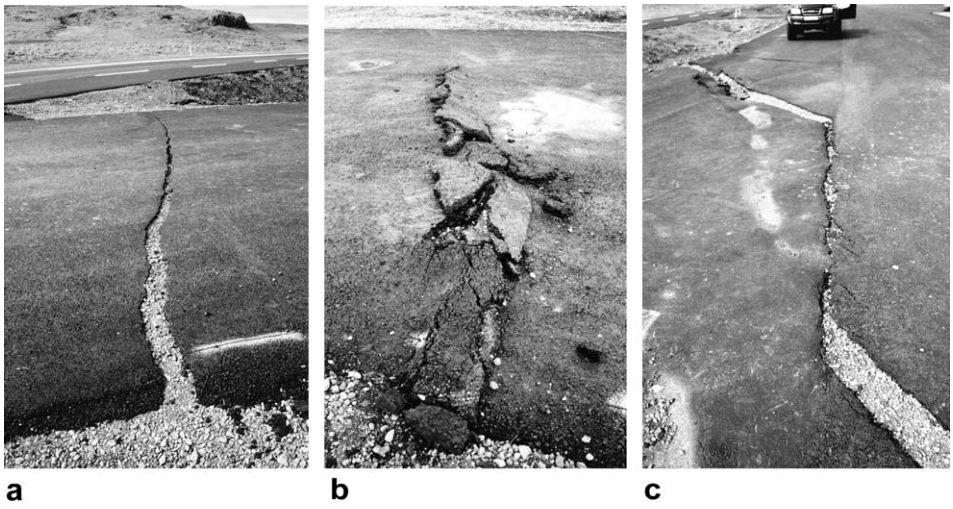

Fig. 4. Photographs of typical brittle features of the 21 June 2000 earthquake in the asphalted car park surface (for location and orientation, see Fig. 3b). (a) Open fissure (referred to as 5 in Fig. 7). (b) Pressure ridge (referred to as 3 in Fig. 8). (c) Left-lateral shear line connecting open fissures (referred to as 4 in Fig. 6).

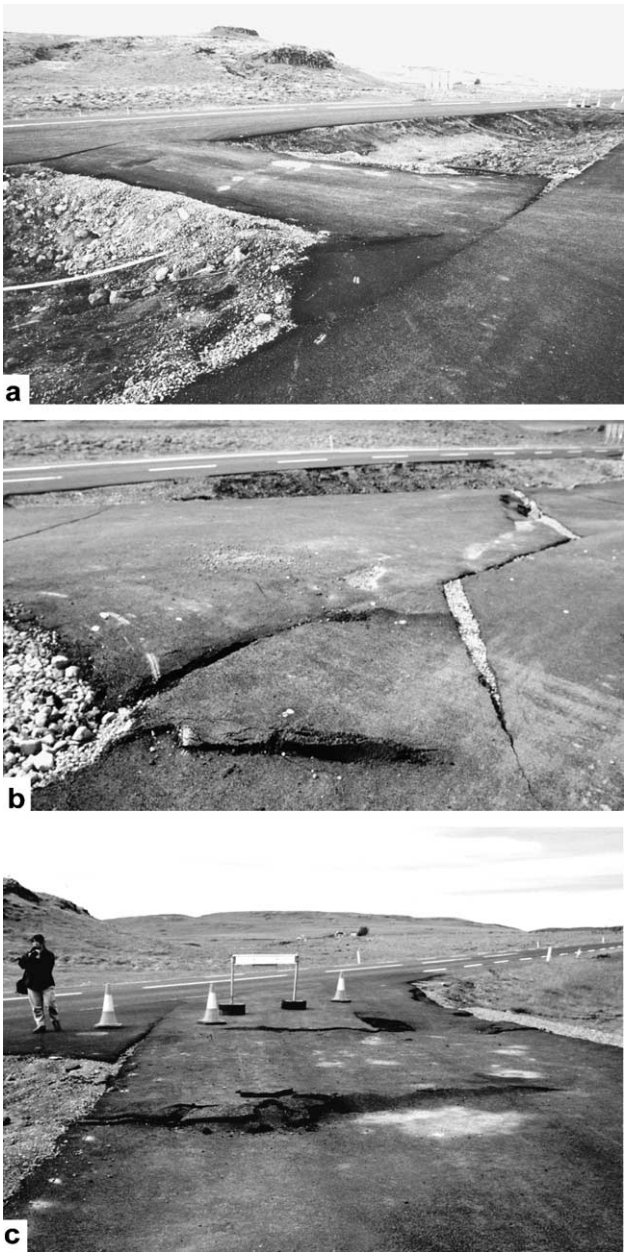

Fig. 5. Photographs of the three sub-areas of asphalted car park surface broken by the 21 June 2000 earthquake (for location and orientation, see Fig. 3b). (a) Central access road (view from NE to SW, map in Fig. 6). (b) Eastern access road (view from NE to SW, map in Fig. 7). (c) Western access road (view from NE to SW, map in Fig. 8).

sub-areas are analysed separately (Figs. 6–8; location in the map of Fig. 3b).

3. Deformation pattern

The distribution of open fractures and thrust ridges in the central access road (Fig. 6) is characterised by a centre of symmetry. The tension fissures are located at the NW and SE corners of this rectangular asphalt road segment, whereas the pressure ridges or highs occur at the opposite, NE and SW, corners (Fig. 6a). This distribution indicates left-lateral shear and rotation of the N–S-trending asphalt access road (Fig. 6b). It is even possible to quantify the deformation, based on serial measurements of the trends and amounts of opening across the open fractures (Fig. 6c).

The two open fractures are 4–5 am long. Their largest dilation is located along the edge of the access road (western and eastern for the northern and southern fractures, respectively). The amount of dilation continuously decreases inside the asphalt surface and vanishes at the opposite tip of the fissure. The trends and the amounts of opening could be accurately measured by matching the irregularities of fissure edges at several places along the fissures. Both the trends and the amplitudes of the relative displacement vectors were thus determined, as shown in Fig. 6c. Because the position of each vector along the fracture was also noted, the variation in opening as a function of the along-fracture position could be analysed. The data showed that this along-fracture variation of dilation is nearly linear. This indicates that the rectangular asphalt access road, bounded by deformation zones at its northern and southern tips, behaves as a rigid plate. The fissure dilation increases in opposite directions for these two fractures, indicating consistent anticlockwise rotation (Fig. 6). It is easy to quantify the rotation through a least-square adjustment of these vectors (in other words, one reconstructs for each fissure the pole of rotation between two rigid bodies). With the data illustrated in Fig. 6c, one obtains consistent values around 3° for open fractures 1 and 2. This indicates that the access road underwent anticlockwise rotation of about 3° during the 21 June earthquake. Then, knowing that this N–S elongated rectangular access road is almost 9 m long, the amount of left-lateral displacement in the E–W direction is easily estimated as the product of this length by the angle in radians, giving a value of 0.46 m (Fig. 6b).

The pattern of brittle features in the eastern, NW–SE-trending access road is more complex (Fig. 7). Three main open fractures were measured. Two of these fissures (3 and 5 in Fig. 7a) trend NE–SW and cut across the car park area and the access road, respectively. The remaining fissure has three separate segments, located at both tips of the left-lateral shear line (Figs. 4c and 5b). The two widest segments (4a and b in Fig. 7a) strike NE–SW at the two tips of, and in close connection with, the E–W shear line. Several minor fissures that also strike NE–SW are arranged en échelon along the shear line. Most displacement vectors of this fissure system trend approximately E–W (Fig. 7c), revealing consistency with E–W left-lateral slip along the shear line. The third segment (4c in Fig. 7a) strikes E–W and was inherited from the same line of mechanical weakness in the asphalt cover as for the shear line, as discussed before (Fig. 5b). Two pressure ridges locally occur, indicating NE–SW shortening. The geometry of this tension-shear pattern indicates a left-lateral slip of about 0.4 m, related to a NW–SE opening of about 0.25 m and an anticlockwise rotation of 2° on average.

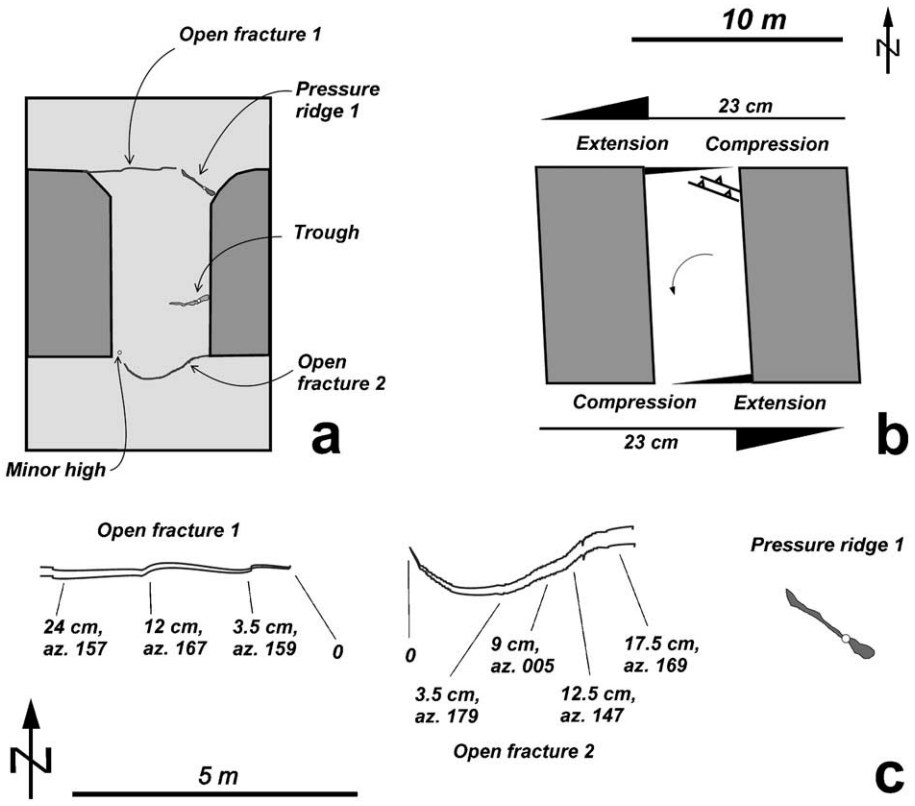

Fig. 6. 21 June 2000 deformation of the central sub-area (location in Fig. 3b). (a) General map obtained with a GPS differential system. Grassy soil and gravel layer in dark grey, asphalted area in light grey, fractures and open fissures as thin lines, pressure ridges as elongated dark areas, pressure ridge top or trough bottom shown as small open dots. (b) Deformation pattern, explanation in text. (c) Relative displacement across fractures (amplitude and azimuth in degrees indicated).

The contribution of tension fractures located on both sides of the tension-shear system (3 and 5 in Fig. 7a) must be added to determine the total deformation. Typically, the trend of fissure opening in this system markedly deviates clockwise from the E–W direction and tends to become NW–SE as the distance to the E–W shear line increases (Fig. 7c). Accordingly, the trend of opening is also NW–SE for the two fissures located away from the shear zone. According to the data shown in Fig. 7c, these fractures accommodate a NW–SE opening of 0.06 m and an anticlockwise rotation of 1°. Note that because the dilation across these tension fractures decreases to zero in opposite directions, the moment of rotation of the deformed plate between them is consistent and anticlockwise, compatible with the left-lateral shear.

All these data indicate that the total rotation of the asphalt layer at the junction between the car park area and the eastern access road is 3° anticlockwise while the NW–SE dilation reaches 0.3 m. The most reliable estimate of left-lateral displacement in this area is given by summing up the E–W opening of the central fissure system in the vicinity of the shear line (0.38 m on average) and the E–W component of dilation across the other fissures (about 0.04 m), giving a total of about 0.42 m (Fig. 7b). This amount of left-lateral shear in the E–W direction is consistent with the estimate of 0.46 m obtained from reconstruction in Fig. 6.

The brittle pattern observed in the western access road differs from those of the other two access roads, because it shows little rotation and horizontal simple shear (Fig. 8). Two open fissures reveal minor rotation (about 2° together). The deformation is dominated by pure shear, with NE–SW elongated tension fissures and a trough, indicating transverse dilation of the access road, and NW–SE-trending pressure ridges revealing along-strike shortening (Fig. 8a and b). The amounts cannot be estimated because it was unclear whether some of the brittle features were a consequence of ground collapse, or damage by vehicles passing through after the earthquake. However, a shortening of 0.4 m could be measured across one of the two pressure ridges (Fig. 8c), giving a lower bound for the NE–SW shortening, and the NW–SE dilation is certainly larger than 0.3 m. Thus, the amount of left-lateral displacement in the E–W direction cannot be smaller than 0.5–0.6 and 0.4–0.5 m, the minimum required to account for the observed NE–SW shortening and NW–SE dilation. This result is compatible with the previous estimates of left-lateral motion obtained in the two sub-sites to the east (Figs. 6 and 7), although it suggests a slightly larger amount of left-lateral displacement.

To summarise, the behaviour of the three asphalted access roads during the earthquake was strongly dependent

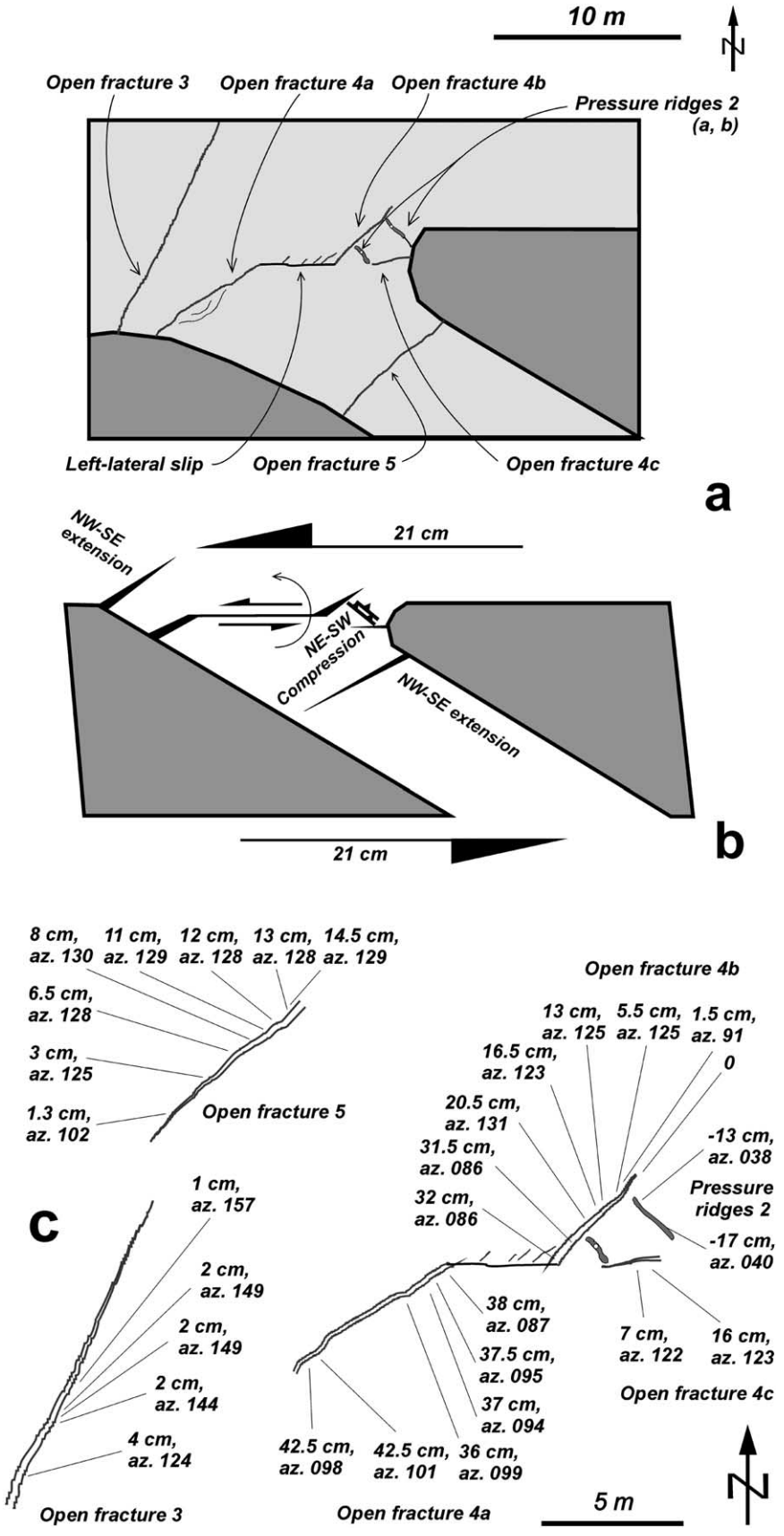

Fig. 7. 21 June 2000 deformation of the eastern sub-area. Caption as for Fig. 6.

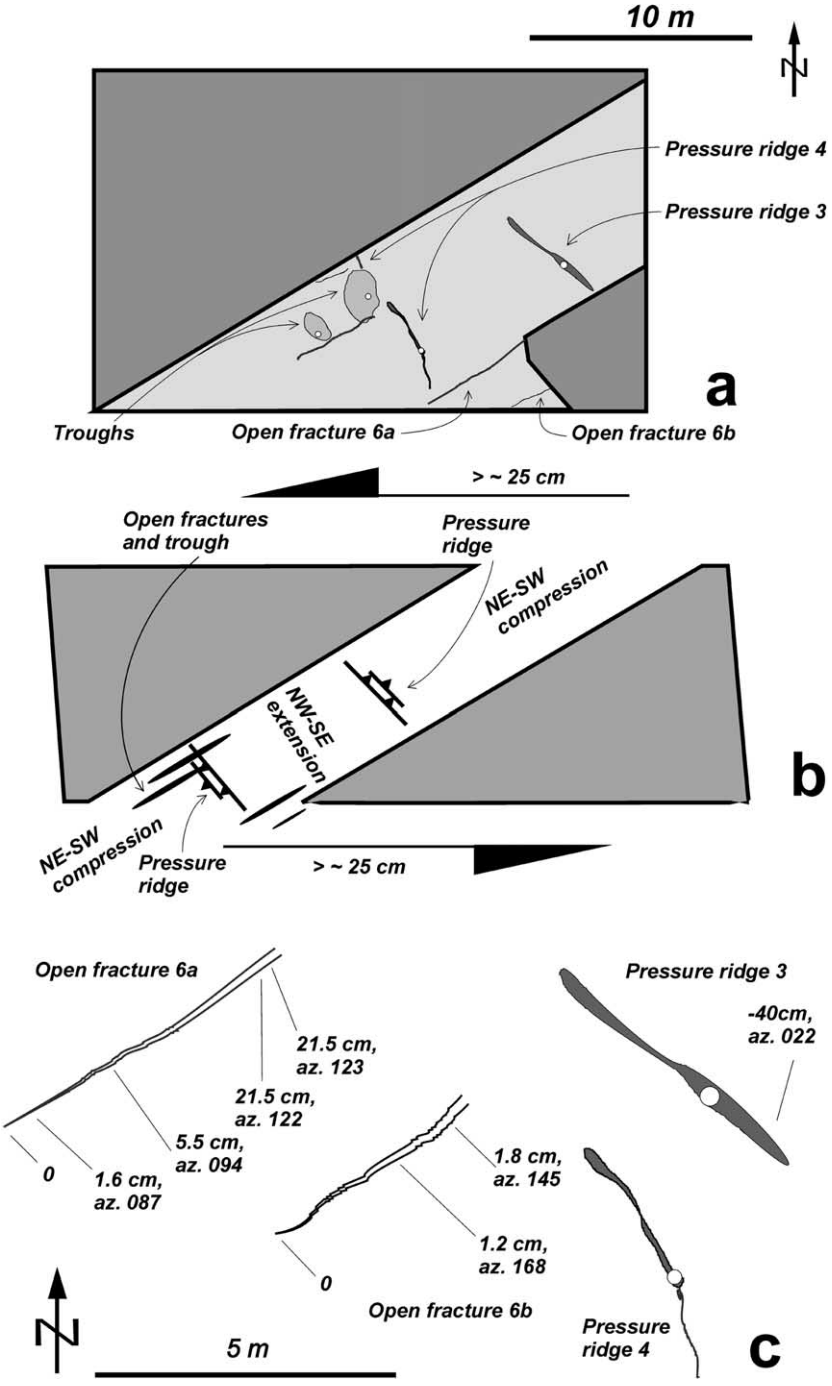

Fig. 8. 21 June 2000 deformation of the western sub-area. Caption as for Fig. 6.

on their orientation relative to the rupture trace (Fig. 3b). The central access road, which trends almost perpendicular to the rupture trace, reveals central symmetry and anticlockwise rotation, with nearly equal contribution of compression and tension structures (Fig. 6). The other two access roads trend obliquely at angles of about 30° to the rupture trace, but in opposite senses (Fig. 3b). Typically, dilation prevails in the eastern, NW–SE-trending access road (Fig. 7), whereas pressure ridges are well-developed in the western, NE–SW trending access road (Fig. 8).

We conclude that the pattern of brittle deformation in the asphalted car park area near Bitra reveal high geometrical and mechanical consistency, indicating that the deformation is dominated by horizontal simple shear along the N80°E direction, with a left-lateral displacement of 40–50 cm during the 21 June 2000 earthquake of southern Iceland. This value is generally consistent with, but somewhat smaller than, the left-lateral offset of 50–60 cm in the N50-60°E direction estimated farther west, in the area of Fig. 2. This variation may suggest that the offset of the Bitra fault

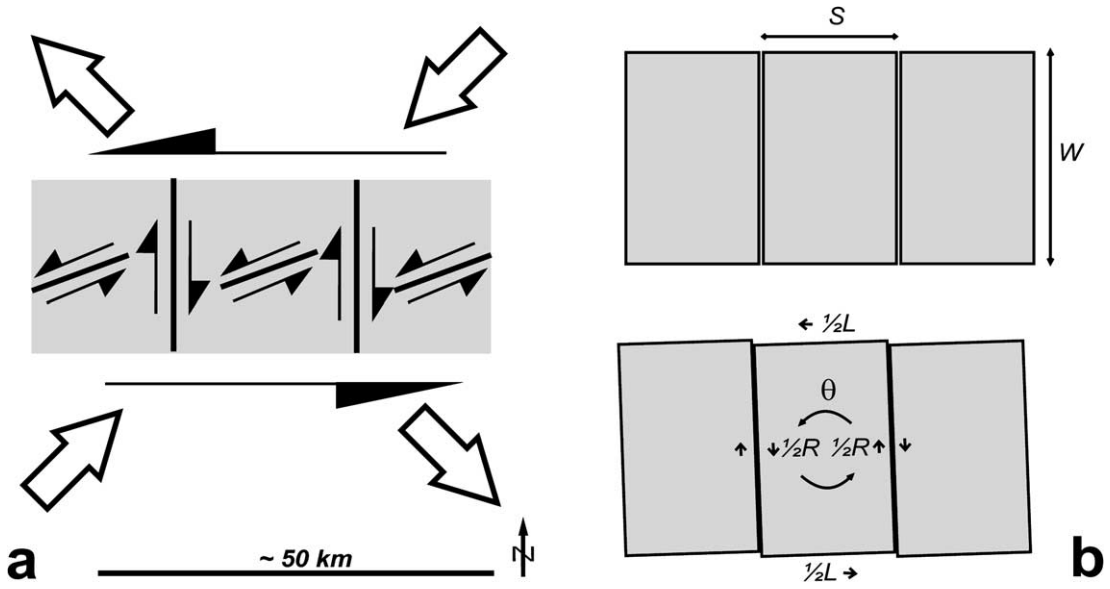

Fig. 9. Fault pattern and mechanisms of the South Iceland Seismic Zone. (a) Distribution of strike-slip movements and far-field stress. Deformed South Iceland Seismic Zone in light grey pattern. Pairs of large open arrows indicate the directions of compression (convergent arrows) and extension (divergent arrows). Couples of black arrows indicate the direction and sense of shear. (b) Determination of the relationships between the width, W, of the deformed zone, the spacing, S, between the N–S right-lateral faults, the anticlockwise rotation angle, θ, of the blocks, the amount of right-lateral slip, R, on N–S faults and the amount of left-lateral slip, L, along the deformation zone.

decreases from west to east in the area studied and that this particular rupture trace of the 21 June earthquake vanishes at a short distance to the east.

4. Discussion and conclusion

Our reconstruction reveals co-seismic left-lateral slip of about 0.5 m along a N80°E-trending fault. The orientation and sense of motion may seem surprising in light of the general behaviour of the 21 June 2000 rupture trace, which trends N–S and reveals right-lateral strike-slip. At Bitra, the nearly E–W main fault trace shown in Fig. 3b is actually a conjugate segment of the main rupture trace (Fig. 1c), which explains both its different orientation and its opposite sense of motion (Fig. 9a).

According to the Icelandic Meteorological Office (2000), the 21 June earthquake, which resulted in the brittle deformation described above, occurred at a depth of about 5 km and the aftershocks revealed a N–S-trending, nearly vertical fault 18 km long reaching a depth of 8 km. The surface fissures mapped by the National Energy Authority of Iceland (2000) occur in a N–S-trending, 23-km-long elongated zone. Both the determination of the focal mechanisms, the distribution of aftershocks and the observation of rupture traces indicate right-lateral motion along this N–S trend (Stefánsson et al., 2000).

According to the same sources, the 17 June 2000 earthquake occurred at a depth of about 6 km on a N–S-trending, 16-km-long, nearly vertical fault reaching a depth of 10 km, as indicated by the aftershocks. The surface fissures occur in a N–S-trending, 24-km-long elongated zone. Right-lateral motion along this N–S trend is revealed by focal mechanisms, aftershock distribution and rupture traces. These two large earthquakes, which occurred within a few days, were thus nearly identical in magnitude, depth, fault extent and orientation, and in mechanism as well. However, they took place on different fault lines, at an E–W distance of about 17 km (Fig. 1b): the Árnes Fault for the 17 June earthquake and the Hestfjall Fault for the 21 June earthquake (Fig. 1c).

A surprising feature of the left-lateral motion of the South Iceland Seismic Zone, a major transform zone between the Reykjanes Ridge and the rift of eastern Iceland (Fig. 1a), is that it is principally accommodated by right-lateral displacement on N–S-trending seismic faults (Einarsson et al., 1981). This observation is supported by seismological observation for the Present (Rögnvaldsson and Slunga, 1994), historical seismicity and paleo-seismicity studies for the Holocene (e.g. Bjarnasson et al., 1993; Bergerat et al., 2002, for two large N–S dextral faults east of the region studied herein), geological mapping (Saemundsson and Einarsson, 1980; Johannesson et al., 1990) and tectonic analysis for the Pleistocene (Passerini et al., 1990; Gudmundsson and Brynjolfsson, 1993; Gudmundsson, 1995; Bergerat et al., 1998, 1999; Bergerat and Angelier, 2000). The 17 and 21 June 2000 earthquakes fit very well in this general scheme.

Before the June 2000 earthquakes, the absence of major left-lateral slip along directions close to E–W was certainly surprising, considering the regional pattern of left-lateral transform motion along an E–W trend (Fig. 9a). In this respect, the existence of left-lateral displacement on faults

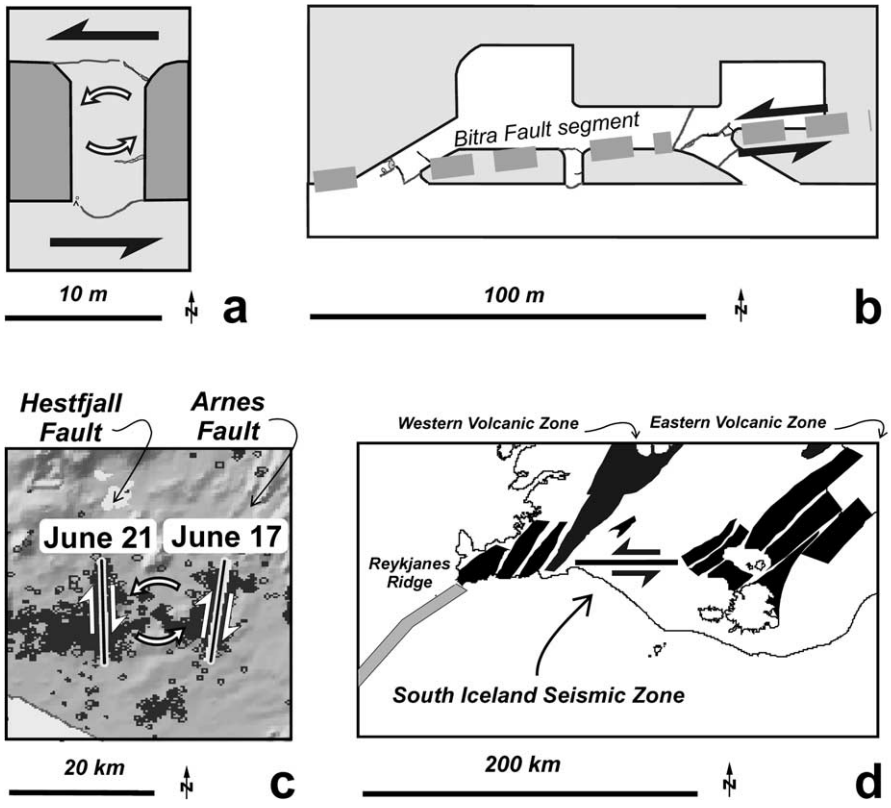

Fig. 10. The multiscale pattern of deformation in the South Iceland Seismic Zone. (a) Anticlockwise rotation of asphalted access road, about 10 m long, related to left-lateral shear (see Fig. 6). (b) Left-lateral motion of the Bitra Fault segment (several hundred metres long). (b) Right-lateral displacement on two major N–S faults of the South Iceland Seismic Zone, approximately 20 km long, and inferred anticlockwise block rotation (see Fig. 9). (c) Left-lateral motion of the South Iceland Seismic Zone, approximately 100 km long.

that trend E–W to NE–SW, such as in Bitra, is significant. Despite the small size of these faults as compared with the N–S-trending ones (Fig. 1c), it shows that faults that directly reflect the overall kinematics of the South Iceland Seismic Zone actually exist. These left-lateral faults are documented not only at Bitra in the Hestfjall Fault zone for the 21 June earthquake, but also at other localities including sites in the Árnes Fault zone for the 17 June earthquake (Bergerat and Angelier, 2001).

These ENE–WSW-trending sinistral faults, like the larger N–S-trending dextral faults, should thus be regarded characteristic of the South Iceland Seismic Zone. The two sets of faults form a conjugate system of N0-30°E faults and N50-80°E left-lateral faults, consistent with a regional stress pattern dominated by NW–SE extension and NE–SW compression, as shown in Fig. 9a. In addition, the ENE–WSW left-lateral strike-slip faults can be regarded as Riedel shears related to the left-lateral transform motion within the E–W-trending South Iceland Seismic Zone (Fig. 9a). In this respect, there is a consistency between our data and the older fault patterns revealed by tectonic analyses in the same region (Bergerat et al., 1999).

Given that the main pattern of active faults is characterised by N–S-trending faults, the left-lateral strike-slip along the South Iceland Seismic Zone can be accounted for by right-lateral motion on these faults in conjunction with block rotation (Fig. 9b). The hypothesis of N–S dextral faults associated with anticlockwise block rotation has already been proposed, in terms of bookshelf-like tectonics, before the June 2000 earthquakes (Einarsson et al., 1981; Einarsson and Eiriksson, 1982; Einarsson, 1991; Sigmundsson et al., 1995). This hypothesis has also been questioned (Gudmundsson, 1995), and despite poor age constraints, the analysis of fault patterns in the Pleistocene failed to reveal large rotations (Bergerat et al., 1999).

In the case of the Árnes and Hestfjall fault zones activated during these earthquakes, the N–S length is 17 km on average according to the distribution of aftershocks, but reaches 25 km on average based on surface traces (Fig. 1c). The E–W spacing between these two faults averages 17 km. It is thus reasonable to consider that these faults bound a rectangular block 25 km long and 17 km wide. Similar blocks can be delineated in other regions along the South Iceland Seismic Zone. The distribution of the seismic activity suggests that the width of the deformation zone averages 20–30 km (Stefánsson et al., 1993; Bödvarsson et al., 1996). It should also be kept in mind that in this region, the shear deformation is accommodated in a brittle mode inside a thin and relatively young basaltic crust overlying a hot ductile mantle, which explains why the left-lateral shear does not

concentrate on a major E–W fault zone but affects a wide elongated zone, at least 20 km wide (in grey pattern in Fig. 9a).

The right-lateral displacement along the N–S direction has been estimated based on the seismological records for the 17 and 21 June 2000 earthquakes and is close to 1 m in both these cases (Icelandic Meteorological Office, 2000; Stefánsson et al., 2000). Because the co-seismic displacement and rotation are very small with respect to the fault length and spacing, the amount of anticlockwise rotation, θ, is simply given by $R = S\theta$, where R is the amount of right-lateral slip and S the spacing between the faults (Fig. 9b). With 17 km for S and 1 m for R, one obtains a value of 6×10^{-5} radians for θ. The amount of left-lateral slip along the E–W direction, L, is then estimated. This amount is given by $L = W\theta$, where W is the width of the zone where the blocks rotate, or the N–S dimension of the rectangular block (Fig. 9b). With the value of θ already obtained and 25 km for S, one obtains a value of 1.5 m for L (with $S = 17$ km as suggested by the aftershock distribution, one would obtain the same value as for R, that is 1 m). Whereas the fault spacing, S, is accurately known based on fault trace mapping, the real value of W is subject to large uncertainty. This is because one ignores the location and size of the area where the rotation is accommodated by internal deformation at the northern and southern boundaries of the block, and hence the N–S extent of the block that can be regarded rigid in the approximation of Fig. 9b.

The bounds of 1–1.5 m for the E–W displacement associated with these two earthquakes should be considered reasonable in light of the general kinematics of the South Iceland Seismic Zone. The velocity of plate separation in Iceland is about 2 cm/year in the N105°E direction (DeMets et al., 1994). Let us assume that the velocity of left-lateral transform motion along the South Iceland Seismic Zone is 1–2 cm/year between the Western and Eastern Volcanic Zones. This represents 50–100% of the relative motion of the plates, depending on how much displacement is absorbed in the Western Volcanic Zone (Fig. 1a). This conjecture is supported by recent geodetic data suggesting that most of the plate divergence occurs in the Eastern Volcanic Zone (Sigmundsson et al., 1995). In terms of long-term movement, a left-lateral displacement of 1–1.5 m is thus obtained after a time span of 50–150 years, which is quite acceptable in light of the average seismic cycle in the South Iceland Seismic Zone (Stefánsson and Halldórsson 1988; Einarsson, 1991).

One may observe that according to the model of Fig. 9b and our estimate of the rotation velocity (about 6×10^{-5} radians in 50–150 years), large rotations would be predicted for longer periods because the transform zone certainly exists since more than about 1 Ma. With the velocity of 10–20 km/Ma considered above, left-lateral simple shear uniformly distributed in a 20 km wide E–W-trending deformation zone results in a shear angle as large as 27-45° in 1 Ma, and depending on the structural pattern still larger physical rotations may be expected. This simple geometrical reasoning, however, is not valid because the South Iceland Seismic Zone has not yet reached a stage of structural maturity as a transform zone (Bergerat and Angelier, 1999). As a consequence, the present-day pattern of faulting (Fig. 9a) and block rotation (Fig. 9b) cannot be extrapolated as it is in the past or the future.

In a system of blocks undergoing faulting and rotation (Fig. 9), one may expect large reorganisation of the fault patterns to occur periodically, as a function of the increasing displacement. As a consequence, estimating the amounts of block rotation would require a knowledge of the structural pattern history far better than that presently available. It should be noted, also, that because of volcanic activity, the Pliocene and Early Pleistocene structural history is commonly hidden in the deformed South Iceland Seismic Zone. This makes any detailed reconstruction of the early Quaternary structural pattern hypothetical, although there is some evidence for a fault system similar to that of the present-day (Bergerat et al., 1999).

It is finally interesting to point out that to some extent the behaviour of the 9-m-long central access road of the car park near Bitra resembles that of the 17–25-km-long blocks separated by the N–S-trending earthquake faults (compare Fig. 10a and c). In both these cases an E–W left-lateral shear is accommodated by the anticlockwise rotation of a block of thin, relatively rigid material (the asphalt layer and the basalt crust, respectively). In this respect, the pattern of brittle deformation at Bitra is not only a geological curiosity. It also reflects some typical features of the behaviour of a rigid plate overlying a more deformable medium, and hence can be regarded as a physical analogue model. This comparison should not be carried too far, particularly because along the E–W direction the asphalt access road has free edges (Fig. 10a), whereas the crustal blocks are in close contact (Fig. 9b). The anticlockwise rotational expression of the left-lateral shear is, however, comparable.

Despite the difference in scale, the anticlockwise rotation of the access road reflects the E–W left-lateral shear of the rupture trace segment (compare Fig. 10a and b). Likewise, the anticlockwise rotation of the crustal blocks reflects the E–W left-lateral shear of the South Iceland Seismic Zone (compare Fig. 10c and d). Note, however, that this rotation is accompanied by N–S right-lateral faulting. The association of anticlockwise rotation and right- and left-lateral movements is accounted for by a model including conjugate and Riedel shear systems (Fig. 9). This structural pattern resembles that of some physical analogue models, in agreement with the brittle behaviour of the thin basaltic crust overlying hot mantle in an area of positive thermal anomaly, as pointed out by many authors (Tryggvason, 1974; Stefánsson and Halldórsson, 1988). Thus, within the South Iceland Seismic Zone, different senses of shear may prevail at different scales (Fig. 10): ENE–WSW left-lateral shear at the scale of few hundred metres (the Bitra fault segment), N–S right-lateral shear at the scale of a few tens of

kilometres (the Árnes Fault and the Hestfjall Fault) and E-W left-lateral shear at the scale of a few hundred kilometres (the entire South Iceland Seismic Zone).

Acknowledgements

The research was supported by the European Commission (project SMSITES, contract EVR1-CT-1999-40002), the French Polar Institute (IFRTP, project 316) and the "Institut Universitaire de France" (IUF). The authors warmly thank A. Gudmundsson for his help while searching for earthquake rupture traces and R. Stefánsson for seismological information, as well as G.O. Fridleifsson and an anonymous referee for useful suggestions.

References

Bergerat, F., Angelier, J., 1999. Géométrie des failles et régimes de contraintes à différents stades de développement des zones transformantes océaniques: exemple de la Zone Sismique Sud-Islandaise et de la Zone de Fracture de Tjörnes (Islande). Comptes Rendus de l'Académie des Sciences, Paris, Sci. Terre & Planètes 329, 653–659.

Bergerat, F., Angelier, J., 2000. The South Iceland Seismic Zone: tectonic and seismotectonic analyses revealing the evolution from rifting to transform motion. Journal of Geodynamics 29, 211–231.

Bergerat, F., Angelier, J., 2001. Mécanismes des failles des séismes des 17 et 21 Juin 2000 dans la Zone Sismique Sud-Islandaise d'après les traces de surface des failles d'Árnes et de l'Hestfjall). Comptes Rendus de l'Académie des Sciences, Paris, Sci. Terre & Planètes 333, 35–44.

Bergerat, F., Gudmundsson, A., Angelier, J., Rögnvaldsson, S.Th., 1998. Seismotectonics of the central part of the South Iceland Seismic Zone. Tectonophysics 298, 319–335.

Bergerat, F., Angelier, J., Verrier, S., 1999. Tectonic stress regimes, rift extension and transform motion: the South Iceland Seismic Zone. Geodinamica Acta 12, 303–319.

Bergerat, F., Angelier, J., Gudmundsson, A., Torfason, H., 2002. Push-ups, fracture patterns, and paleoseismology of the Leirubakki Fault, South Iceland. Journal of Structural Geology, accepted for publication.

Bjarnasson, I.Th., Cowie, P., Anders, M.H., Seeber, L., Scholz, C.H., 1993. The 1912 Iceland earthquake rupture: growth and development of a nascent transform system. Bulletin of the Seismological Society of America 83, 416–435.

Bödvarsson, R., Rögnvaldsson, S.Th., Jakobsdottir, S.S., Slunga, R., Stefánsson, R., 1996. The SIL Data Acquisition and Monitoring System. Seismological Research Letters 67, 35–46.

DeMets, C., Gordon, R.G., Argus, F., Stein, S., 1994. Effect of recent revisions to the geomagnetic reversal time-scale on estimates of current plate motion. Geophysical Research Letters 21, 2191–2194.

Einarsson, P., 1991. Earthquake and present-day tectonism in Iceland. Tectonophysics 189, 261–279.

Einarsson, P., Eiriksson, J., 1982. Earthquake fractures in the districts Land and Rangárvellir in the south Iceland seismic zone. Jökull 32, 113–120.

Einarsson, P., Björnsson, S., Foulger, G., Stefánsson, R., Skaftadottir, Th., 1981. Seismicity pattern in the South Iceland Seismic Zone. In: Simpson, D.W., Richards, P.G. (Eds.), Earthquake Prediction: An International Review. AGU Maurice Ewing Series 4, Washington D.C., pp. 141–151.

Gudmundsson, A., 1995. Ocean-ridge discontinuities in Iceland. Journal of the Geological Society, London 152, 1011–1015.

Gudmundsson, A., Brynjolfsson, S., 1993. Overlapping rift-zone segments and the evolution of the South Iceland Seismic Zone. Geophysical Research Letters 201, 903–906.

Icelandic Meteorological Office (Vedurstofa íslands), 2000. Department of Geophysics, Internet site at address http://hraun.vedur.is/ja/englishweb/index.html.

Johannesson, H., Jakobsson, S.P., Saemundsson, K., 1990. Geological map of Iceland, sheet 6, south Iceland, Icelandic Museum of Natural History and Iceland Geodetic Survey, Reykjavik.

National Energy Authority of Iceland (Orkustofnun), 2000. Geosciences Division, Internet site at address http://www.os.is/english/.

Passerini, P., Sguazzoni, G., Marcucci, M., Zan, L., 1990. Slickensides in western and Southern Iceland: data from Langavatn, Burfell and Vördufell. Ofioliti 15, 191–196.

Passerini, P., Marcucci, M., Sguazzoni, G., Pecchioni, E., 1997. Longitudinal strike-slip faults in oceanic rifting: a mesostructural study from western to southeastern Iceland. Tectonophysics 269, 65–89.

Roberts, D., 2000. Pull-apart stepover structures in an asphalted road surface—a geological curiosity. Journal of Structural Geology 22, 1469–1472.

Rögnvaldsson, S., Slunga, R., 1994. Single and joint fault plane solutions for microearthquakes in South Iceland. Tectonophysics 237, 73–86.

Saemundsson, K., Einarsson, S., 1980. Geological map of Iceland, sheet 3, southwest Iceland, Icelandic Museum of Natural History and Iceland Geodetic Survey, Reykjavik.

Sigmundsson, F., Einarsson, P., Bilham, R., Sturkell, E., 1995. Rift-transform kinematics in south Iceland: deformation from Global Positioning System measurements, 1986 to 1992. Journal of Geophysical Research 100, 6235–6248.

Stefánsson, R., Halldórsson, P., 1988. Strain release and strain build-up in the south Iceland seismic zone. Tectonophysics 152, 267–276.

Stefánsson, R., Bödvarsson, R., Slunga, R., Einarsson, P., Jakobsdottir, S.S., Bungum, H., Gregersen, S., Havskov, J., Hjelme, J., Korhonen, H., 1993. Earthquake prediction research in the South Iceland Seismic Zone and the SIL project. Bulletin of the Seismological Society of America 83 (3), 696–716.

Stefánsson, R., Gudmundsson, G.B., Halldórsson, P., 2000. The two large earthquakes in the South Iceland seismic zone on June 17 and 21, 2000. Internet site at address http://vedur.is.

Tryggvason, E., 1974. Surface deformation in Iceland and crustal stress over a mantle plume. In: Thost-Christensen, A. (Ed.). Continuum Mechanics Aspects of Geodynamics and Rock Fracture Mechanics. Reidel, Dordrecht, pp. 245–254.

University of Iceland (Verkfraedistofnun Háskóla íslands), 2000. Earthquake Engineering Research Center. Internet site at address http://www.afl.hi.is.

Ward, P.L., 1971. New interpretation of the geology of Iceland. Geological Society of America Bulletin 82, 2991–3012.